Direct Power Control of DFIG With Constant Switching Frequency and Improved Transient Performance

Dawei Zhi, *Student Member, IEEE*, and Lie Xu, *Senior Member, IEEE*

***Abstract*—This paper proposes a new direct power control (DPC) strategy for a doubly fed induction generator (DFIG)-based wind turbine system. The required rotor control voltage, which eliminates active and reactive power errors within each fixed time period, is directly calculated based on stator flux, rotor position, and active and reactive powers and their corresponding errors. No extra power or current control loops are required, simplifying the system design, and improving transient performance. Constant converter switching frequency is achieved that eases the design of the power converter and the ac harmonic filter. Rotor voltage limit during transients is investigated, and a scheme is proposed that prioritizes the active and reactive power control such that one remains fully controlled while the error of the other is reduced. The impact of machine parameter variations on system performance is investigated and found negligible. Simulation results for a 2 MW DFIG system demonstrate the effectiveness and robustness of the proposed control strategy during variations of active and reactive power, machine parameters, and wind speed.**

***Index Terms*—Constant switching frequency, DFIG, direct power control, pulse width modulation (PWM) converter, wind energy.**

NOMENCLATURE

θ_s, θ_r	Stator flux, rotor angles in the stationary frame.
θ	Phase angle between the rotor and stator flux vectors.
$\omega_1, \omega_r, \omega_s$	Synchronous, rotor, slip angular frequency.
$\boldsymbol{\psi}_s, \boldsymbol{\psi}_r$	Stator, rotor flux vectors.
$\boldsymbol{I}_s, \boldsymbol{I}_r$	Stator, rotor current vectors.
L_m	Mutual inductance.
$L_{\sigma_s}, L_{\sigma_r}$	Stator, rotor leakage inductance.
L_s, L_r	Stator, rotor self-inductance.
R_s, R_r	Stator, rotor resistance.
P_s, Q_s	Stator active and reactive power.
$\boldsymbol{V}_s, \boldsymbol{V}_r$	Stator, rotor voltage vectors.
Superscripts	
s	Synchronous reference frame.
r	Rotor reference frame.
$*$	Reference value.
$\hat{}$	Conjugate complex.
Subscripts	
α–β	α–β axis.
s, r	Stator, rotor.
d, q	Synchronous d–q axis.

Manuscript received June 29, 2006; revised October 16, 2006. Paper no. TEC-00227-2006.

The authors are with the School of Electronics, Electrical Engineering and Computer Science, Queen's University of Belfast, Belfast BT7 1NN, U.K. (e-mail: dzhi01@qub.ac.uk; l.xu@ee.qub.ac.uk).

Digital Object Identifier 10.1109/TEC.2006.889549

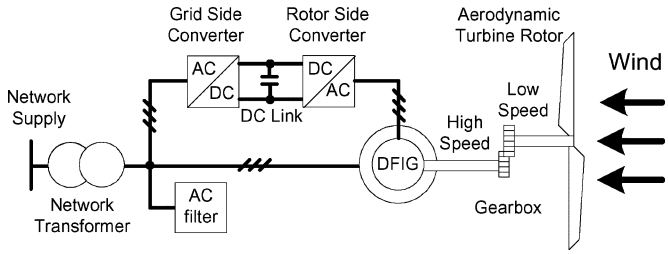

Fig. 1. Schematic of a DFIG-based wind generation system.

I. INTRODUCTION

DOUBLY-fed induction generator (DFIG) wind turbines with converters rated at about 25–30% of the generator rating are becoming increasingly popular. DFIG-based wind turbines offer variable speed operation, four-quadrant active and reactive power capabilities, lower converter cost, and reduced power loss compared to wind turbines using fixed speed induction generators or fully-fed synchronous generators with full-sized converters. A schematic of a DFIG-based wind energy generation system is shown in Fig. 1.

Control of DFIG wind turbine systems is traditionally based on either stator-flux-oriented [1], [2] or stator-voltage-oriented vector control [3], [4]. The scheme decouples the rotor current into active and reactive power components. Control of the active and reactive powers is achieved with a rotor current controller. One main drawback of this system is that its performance depends highly on accurate machine parameters such as stator, rotor resistances, and inductances. Thus, performance degrades when actual machine parameters depart from values used in the control system.

Direct torque control (DTC) of induction machines, developed more than a decade ago, provides an alternative to vector control [5], [6]. DTC minimizes the use of machine parameters and reduces the complexity of vector control algorithms. The DTC method directly controls machine torque and flux by selecting voltage vectors from a look-up-table using the stator flux and torque information. One problem with the basic DTC scheme is that its performance deteriorates during starting and low-speed operations. Methods proposed to address this problem include use of a dither signal [7], a modified switching table to apply available voltage vectors in appropriate sequence [8], or predictive techniques [9]. Another problem for DTC is converter

switching frequency variation that significantly complicates power circuit design. The hysteresis controller bandwidth must be chosen carefully [10] to ensure that the switching frequency stays within the power converter's maximum limit for all operating conditions. Modified DTC strategies, incorporating space vector modulation (SVM), have been used to achieve constant switching frequency [11]–[14]. Inverter switching duty cycles in [11] were calculated directly, based on torque and flux errors within each sample period, whereas in [12] and [13], they are generated from PI controllers. Output voltage vector was selected in [14] using the conventional DTC switching table but the voltage vector duration was determined by the torque-ripple minimum strategy. Although the switching frequencies were constant as those DTC strategies, extra drawbacks were introduced, such as complicated online calculation [11], additional PI controller parameters [12], [13], and weak robustness on machine parameter variations [11]–[14].

Based on the principles of DTC strategy, direct power control (DPC) was developed for three-phase pulse width modulation (PWM) rectifiers [15]–[17]. Converter switching states were selected from an optimal switching table based on instantaneous errors of active and reactive powers and the angular position of converter terminal voltage vector [15], [16], or virtual flux that is the integration of the converter output voltage [17]. More recently, DPC control of DFIG-based wind turbine systems has been proposed [18], [19]. In [18], the control system was based on the estimated rotor flux. Switching vectors were selected from the optimal switching table using the estimated rotor flux position, and the errors of the rotor flux and the active power/torque. The rotor flux reference was calculated using the reactive power/power factor reference. Since the rotor supply frequency, which equals the DFIG slip frequency, can become very low, rotor flux estimation is significantly affected by the machine parameter variations. In [19], a DPC strategy based on the estimated stator flux was proposed. Since the stator (network) voltage is relatively harmonic-free with fixed frequency, a DFIG's estimated stator flux accuracy can be guaranteed. Switching vectors were selected from the optimal switching table using the estimated stator flux position, and the errors of the active power and reactive powers. Thus, the control system is very simple, and the machine parameters' impact on system performance was found to be negligible. However, like a conventional DTC, DPC has switching frequency that varies significantly with active and reactive power variations, machine operating speed (rotor slip), and the power controllers' hysteresis bandwidth [18], [19]. Apart from complicating the converter design, the stator side ac filter (Fig. 1), which prevents switching harmonics from entering the network, needs to be designed to eliminate broadband harmonics. With increased size and power loss, this significantly reduces filter efficiency.

This paper proposes a new DPC control strategy for DFIG-based wind energy generation systems with constant switching frequency and improved transient performance. The method directly calculates required rotor control voltage with each switching period, based on the estimated stator flux, the active and reactive powers, and their errors. A method to limit rotor control voltage and further improve transient performance is described.

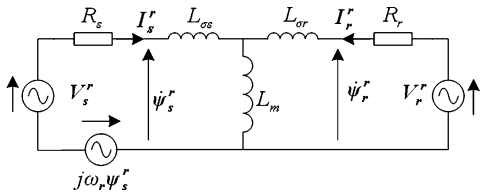

Fig. 2. Equivalent circuit of a DFIG in the rotor reference frame.

The paper is organized as follows. Section III gives an overview of the original DPC strategy for DFIG control and Section IV describes the proposed strategy. Simulation results for a 2 MW DFIG generation system are presented in Section V to demonstrate the performance of the proposed control strategy. Finally, conclusions are drawn in section VI.

II. Principles of DPC for DFIG

In the rotor $\alpha_r-\beta_r$ reference frame rotating at an angular speed of ω_r, Fig. 2 shows the equivalent circuit of a DFIG. According to Fig. 2, the stator voltage vector in the rotor frame is given as

$$V_s^r = R_s I_s^r + \frac{d\psi_s^r}{dt} + j\omega_r \psi_s^r. \tag{1}$$

In the rotor reference frame, the stator and rotor flux are expressed as

$$\begin{aligned} \psi_s^r &= L_s I_s^r + L_m I_r^r \\ \psi_r^r &= L_r I_r^r + L_m I_s^r \end{aligned} \tag{2}$$

where $L_s = L_{\sigma s} + L_m$ and $L_r = L_{\sigma r} + L_m$.

Based on (2), the stator current is given as

$$I_s^r = \frac{L_r \psi_s^r - L_m \psi_r^r}{L_s L_r - L_m^2} = \frac{\psi_s^r}{\sigma L_s} - \frac{L_m \psi_r^r}{\sigma L_s L_r} \tag{3}$$

where $\sigma = (L_s L_r - L_m^2)/L_s L_r$ is the leakage factor.

Referring to [20], the stator active and reactive power inputs from the network can be calculated as

$$P_s - jQ_s = \frac{3}{2} V_s^r \times \hat{I}_s^r. \tag{4}$$

If the network voltage is constant, neglecting the stator resistance, both the amplitude $|\psi_s|$ and the rotating speed ω_1 of the stator flux remain constant [19]. Substituting (1) and (3) into (4) yields the stator active and reactive power inputs [19]:

$$\begin{aligned} P_s &= -k_\sigma \omega_1 |\psi_s||\psi_r| \sin\theta \\ Q_s &= k_\sigma \omega_1 |\psi_s| \left(|\psi_r| \cos\theta - \frac{L_r}{L_m} |\psi_s| \right) \end{aligned} \tag{5}$$

where $k_\sigma = 1.5 L_m/(\sigma L_s L_r)$ and θ is the angle between the rotor and stator flux vectors, as shown in Fig. 3.

Differentiating (5) results in the following:

$$\begin{aligned} \frac{dP_s}{dt} &= -k_\sigma \omega_1 |\psi_s| \frac{d\left(|\psi_r| \sin\theta\right)}{dt} \\ \frac{dQ_s}{dt} &= k_\sigma \omega_1 |\psi_s| \frac{d\left(|\psi_r| \cos\theta\right)}{dt}. \end{aligned} \tag{6}$$

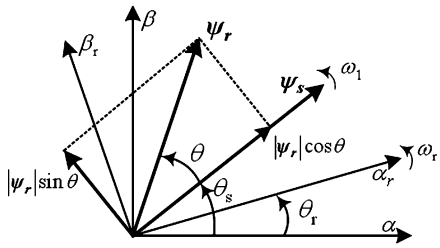

Fig. 3. Stator and rotor flux vectors in stationary and rotor reference frames.

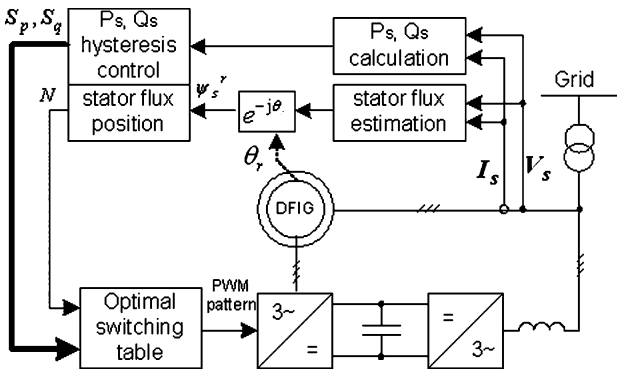

Fig. 4. Schematic of the original DPC control strategy [19].

As $|\psi_s|$ and ω_1 remain constant, (6) indicates that the variations of active and reactive powers can be controlled by varying the rotor flux components $|\psi_r| \sin \theta$ and $|\psi_r| \cos \theta$, respectively. The relationships between $|\psi_r| \sin \theta$ and $|\psi_r| \cos \theta$, the rotor flux, and the stator flux can be seen in Fig. 3.

As shown in Fig. 2, neglecting the rotor resistance, the rotor flux variation in the rotor reference frame can be approximated as

$$\frac{d\psi_r^r}{dt} = V_r^r - R_r I_r^r \approx V_r^r. \tag{7}$$

Equation (7) indicates that the rotor flux change is directly controlled by the applied rotor voltage, i.e., the rotor flux moves in the direction of the applied rotor voltage vector, and its speed is proportional to the amplitude of the voltage vector. For a three-phase two-level converter, the operation of the six power devices results in eight different voltage vectors [21]. Within each sampling period, if the stator flux position is known, the impact of each voltage vector on the variations of the rotor flux, the $|\psi_r| \sin \theta$ and $|\psi_r| \cos \theta$ components can be determined. Consequently, according to (6), the influence of each voltage vector on active and reactive power variations can be calculated. An optimal switching table can, then, be arranged to give the most effective rotor voltage vector to reduce the power errors.

Fig. 4 shows the arrangement of the DPC control strategy proposed in [19]. Hysteresis control of the active and reactive powers within each sampling period is achieved by selecting and applying the optimal rotor voltage vector. In order to guarantee the effective control of the powers, the sampling frequency must be sufficiently high, usually in the range of tens of kilohertz.

The converter's switching frequency depends highly on the operating conditions such as the active and reactive powers, the hysteresis bandwidth, the rotor slip, etc., and can vary significantly [19]. Therefore, it is difficult to evaluate the rotor-side converter's power loss and loading conditions, and to design a suitable cooling system. Furthermore, because of variable switching frequency, the harmonics in the stator current also vary according to the operating conditions. The ac filter has a significantly complicated design, since it has to absorb broadband frequency components to prevent their entering the network.

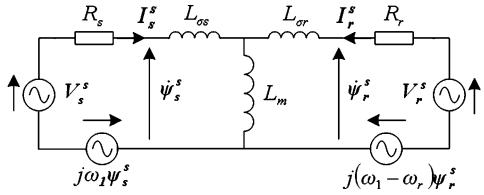

Fig. 5. Equivalent circuit of a DFIG in the synchronous d–q reference frame.

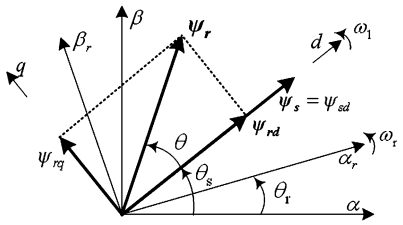

Fig. 6. Stator and rotor flux vectors in the synchronous d–q frames.

III. Proposed DPC Strategy

A. DFIG Representation in the Synchronous Reference Frame

The equivalent circuit of a DFIG in the synchronous d–q frame, rotating at the speed of ω_1, is shown in Fig. 5. The d-axis of the synchronous frame is fixed to the stator flux, as shown in Fig. 6.

According to Fig. 5, the stator voltage vector in the synchronous d–q reference frame is given as

$$V_s^s = R_s I_s^s + \frac{d\psi_s^s}{dt} + j\omega_1 \psi_s^s. \tag{8}$$

Under balanced ac voltage supply, the amplitude and rotating speed of the stator flux are constant. Therefore, in the synchronous d–q frame, the stator flux maintains a constant value. Thus,

$$\begin{aligned} \psi_s^s &= \psi_{sd} \\ \frac{d\psi_s^s}{dt} &= 0. \end{aligned} \tag{9}$$

Considering (9) and neglecting the voltage drop across the stator resistance, (8) can be simplified as

$$V_s^s = j\omega_1 \psi_s^s = j\omega_1 \psi_{sd}. \tag{10}$$

Similar to (3), the stator current in the synchronous d–q frame is given as

$$I_s^s = \frac{L_r \psi_s^s - L_m \psi_r^s}{L_s L_r - L_m^2} = \frac{\psi_s^s}{\sigma L_s} - \frac{L_m \psi_r^s}{\sigma L_s L_r}. \tag{11}$$

Thus, the stator active and reactive power inputs can be calculated as

$$\begin{aligned} P_s - jQ_s &= \frac{3}{2} j\omega_1 \psi_{sd} \times \left(\frac{\hat{\psi}_s^s}{\sigma L_s} - \frac{L_m \hat{\psi}_r^s}{\sigma L_s L_r} \right) \\ &= \frac{3}{2} j\omega_1 \psi_{sd} \times \left[\frac{\psi_{sd}}{\sigma L_s} - \frac{L_m (\psi_{rd} - j\psi_{rq})}{\sigma L_s L_r} \right] \\ &= k_\sigma \omega_1 \left[-\psi_{sd}\psi_{rq} + j\psi_{sd} \left(\frac{L_r \psi_{sd}}{L_m} - \psi_{rd} \right) \right]. \end{aligned} \tag{12}$$

Splitting (12) into real and imaginary parts yields

$$\begin{aligned} P_s &= -k_\sigma \omega_1 \psi_{sd} \psi_{rq} \\ Q_s &= k_\sigma \omega_1 \psi_{sd} \left(\psi_{rd} - \frac{L_r}{L_m} \psi_{sd} \right). \end{aligned} \tag{13}$$

As the stator flux stays constant, according to (13), the active and reactive power changes over a constant period of T_s are given by

$$\begin{aligned} \Delta P_s &= -k_\sigma \omega_1 \psi_{sd} \, \Delta\psi_{rq} \\ \Delta Q_s &= k_\sigma \omega_1 \psi_{sd} \, \Delta\psi_{rd}. \end{aligned} \tag{14}$$

Equation (14) indicates that the stator reactive and active power changes are determined by the changes of the rotor flux components on the d–q axis, i.e., $\Delta\psi_{rd}$ and $\Delta\psi_{rq}$, respectively.

B. Active and Reactive Power Control

The proposed active and reactive power control calculates the required rotor voltage that will reduce the active and reactive power errors to zero during a constant sampling time period of T_s. A PWM modulator is, then, used to generate the applied rotor voltage for the T_s period.

At the beginning of the sampling period T_s, the active and reactive power errors are calculated as

$$\begin{aligned} \Delta P_s &= P_s^* - P_s \\ \Delta Q_s &= Q_s^* - Q_s. \end{aligned} \tag{15}$$

According to (14), in order to reduce the power errors shown in (15) to zero, the rotor flux changes in the d–q axis must follow

$$\begin{aligned} \Delta\psi_{rq} &= -\frac{\Delta P_s}{k_\sigma \omega_1 \psi_{sd}} \\ \Delta\psi_{rd} &= \frac{\Delta Q_s}{k_\sigma \omega_1 \psi_{sd}}. \end{aligned} \tag{16}$$

As shown in Fig. 5, in the synchronous d–q reference frame, the rotor flux is given by

$$\frac{d\psi_r^s}{dt} = V_r^s - R_s I_r^s - j(\omega_1 - \omega_r)\psi_r^s. \tag{17}$$

Neglecting the rotor resistance, within the period of T_s, the changes of rotor flux in the d- and q-axis are given by

$$\begin{aligned} \Delta\psi_{rd} &= V_{rd} T_s + \omega_s \psi_{rq} T_s \\ \Delta\psi_{rq} &= V_{rq} T_s - \omega_s \psi_{rd} T_s \end{aligned} \tag{18}$$

where $\omega_s = \omega_1 - \omega_r$ is the slip frequency.

Combining (16) and (18), within the T_s period, the rotor voltage required to eliminate the power errors in the d–q reference frame is calculated as

$$\begin{aligned} V_{rd} &= \frac{1}{T_s} \frac{\Delta Q_s}{k_\sigma \omega_1 \psi_{sd}} - \omega_s \psi_{rq} \\ V_{rq} &= \frac{1}{T_s} \frac{-\Delta P_s}{k_\sigma \omega_1 \psi_{sd}} + \omega_s \psi_{rd}. \end{aligned} \tag{19}$$

The rotor flux in the d–q frame can be calculated using a method similar to that shown in (2). However, its accuracy could be affected by the variation of L_m as will be discussed later in the paper. An alternative method is based on (13) as

$$\begin{aligned} \psi_{rd} &= \frac{Q_s}{k_\sigma \omega_1 \psi_{sd}} + \frac{L_r}{L_m} \psi_{sd} \\ \psi_{rq} &= \frac{-P_s}{k_\sigma \omega_1 \psi_{sd}}. \end{aligned} \tag{20}$$

Substituting (20) into (19) results in the required rotor voltage in the d–q reference frame as

$$\begin{aligned} V_{rd} &= \frac{1}{T_s} \frac{\Delta Q_s}{k_\sigma \omega_1 \psi_{sd}} + \omega_s \frac{P_s}{k_\sigma \omega_1 \psi_{sd}} \\ V_{rq} &= \frac{1}{T_s} \frac{-\Delta P_s}{k_\sigma \omega_1 \psi_{sd}} + \omega_s \left(\frac{Q_s}{k_\sigma \omega_1 \psi_{sd}} + \frac{L_r}{L_m} \psi_{sd} \right). \end{aligned} \tag{21}$$

The first terms on the right-hand side reduce power errors while the second terms compensate the rotor slip that causes the different rotating speeds of the stator and rotor flux. As can be seen, calculations require only simple multiplications and divisions, and no complicated mathematics.

C. Rotor Output Voltage Limit and PWM Modulation

For a DFIG, the maximum output voltage from the rotor-side converter is usually within the range of 30% of the stator voltage. Under steady-state operation, the required rotor control voltage is unlikely to exceed the voltage limit of the rotor-side converter. However, during transient conditions, large variations of active and/or reactive power references can result in large power errors in one sampling period T_s. Consequently, the rotor voltages V_{rd} and V_{rq}, calculated using (21), may exceed the voltage capability of the converter. Therefore, V_{rd} and V_{rq} must be limited to improve the transient response. In the case of large active power error, the calculated V_{rq} is likely to exceed the voltage limit, while V_{rd} remains within the limit. Traditionally, the two voltage components were scaled proportionally. However, the scaling of V_{rd} in this case could result in reactive power control being temporarily lost. The approach adopted here maintains V_{rd} and scales V_{rq} according to the maximum voltage limit such that reactive power remains controlled while active power is driven toward the desired value. This process can be represented as

$$\begin{aligned} V'_{rd} &= V_{rd} \\ V'_{rq} &= \text{sign}(V_{rq}) \sqrt{V_{r\max}^2 - V_{rd}^2} \end{aligned} \tag{22}$$

where $V_{r\max}$ is the maximum voltage the rotor-side converter can produce.

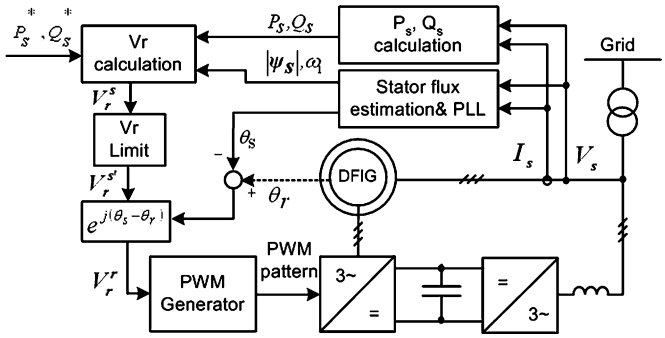

Fig. 7. Schematic of the proposed DPC for a DFIG system.

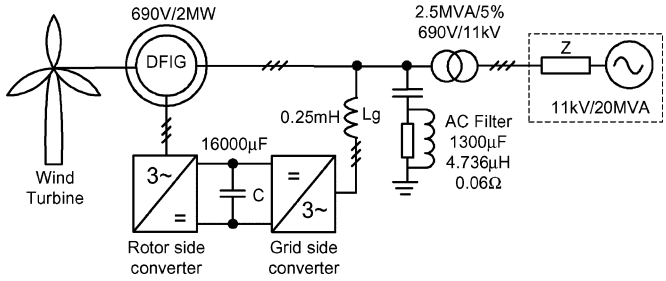

Fig. 8. Schematic of the simulated system.

The opposite is true during reactive power steps when V_{rq} remains unchanged while V_{rd} is scaled. Within the sampling period, if simultaneous step changes of active and reactive powers cause both V_{rd} and V_{rq} to exceed the voltage limit, V_{rd} and V_{rq} are scaled proportionally as

$$V'_{rd} = V_{rd}\frac{V_{r\max}}{\sqrt{V_{rd}^2 + V_{rq}^2}}$$

$$V'_{rq} = V_{rq}\frac{V_{r\max}}{\sqrt{V_{rd}^2 + V_{rq}^2}}. \tag{23}$$

Once the required rotor output voltage in the synchronous reference frame is obtained, it must be transformed to the rotor α_r–β_r reference frame. This is achieved using the following:

$$V_r^r = V_r^s\, e^{j(\theta_s - \theta_r)}. \tag{24}$$

The desired rotor voltage in the rotor frame can, then, generate switching signals for the rotor-side converter using either SVM [21] or sinusoidal PWM [22] whose switching frequency is fixed constantly at $1/(2T_s)$. A typical switching frequency for this converter ranges within a few kilohertz, and therefore, the proposed DPC sampling frequency is within a few kilohertz range.

D. System Implementation

As shown in (21) and (24), to calculate the required rotor voltage, the values of the active and reactive powers and their errors, the stator flux amplitude, rotating speed and angle, and the rotor angle are required.

The stator instant active and reactive powers can be directly calculated from the measured stator voltages and currents. In the stationary reference frame, the stator flux is estimated using the following:

$$\psi_s = \int (V_s - R_s I_s)\, dt. \tag{25}$$

Since the stator voltage is relatively harmonic-free and its frequency is fixed, the previous equation can provide an accurate estimation of the stator flux.

The schematic of the proposed DPC strategy is shown in Fig. 7. The three-phase stator voltages and currents are measured and transformed into the stationary α–β reference frame. The stator active and reactive powers are calculated and the stator flux is estimated. A phase-locked loop (PLL) is, then, used to calculate the stator flux angle θ_s and its rotating speed ω_1. The rotor d–q control voltage references are, then, calculated using (21). They are passed to the voltage limiter and transformed to the rotor frame using the rotor angle that is obtained by a shaft encoder. Finally, PWM switching pattern is generated and used to control the rotor-side converter.

E. Impact of Parameter Variations on System Performance

Stator flux estimation requires knowledge of stator resistance that has negligible impact on system performance [19]. Using (21), rotor voltage calculation accuracy is mainly influenced by the constant k_σ and the inductance ratio L_r/L_m that are determined by the stator and rotor leakage and mutual inductance. Since the leakage flux magnetic path is mainly air, the variation of the leakage inductance during operation is insignificant. However, mutual inductance variation needs to be considered due to possible variation of the magnetic permeability of the stator and rotor cores under different operating conditions. As described in Appendix A, considering the relatively small leakage inductance $L_{\sigma s}$ and $L_{\sigma r}$ compared to the mutual inductance L_m, the required parameters can be simplified as

$$k_\sigma \approx \frac{3}{2}\frac{1}{L_{\sigma s} + L_{\sigma r}}, \frac{L_r}{L_m} = 1 + \frac{L_{\sigma s}}{L_m} \approx 1. \tag{26}$$

As can be seen from (26), the variation of L_m has little impact on k_σ and L_r/L_m, and therefore, its influence on the performance of the proposed control strategy would also be insignificant.

IV. Simulation Results

Simulations of the proposed control strategy for a DFIG-based generation system used PSCAD/EMTDC, and Fig. 8 shows the schematic of the implemented system. The DFIG is rated at 2 MW, and its parameters are given in Appendix B. The nominal converter dc link voltage was set at 1200 V. Based on the proposed DPC strategy, the rotor-side converter controls the DFIG stator's active and reactive power. The sampling period during simulation was 250 μs, which refers to a rotor-side converter switching frequency of 2 kHz. The grid-side converter has to maintain a constant dc link voltage, and it is controlled by a method similar to the dc voltage controller in a VSC transmission system [23] with a switching frequency of 2 kHz. As shown in Fig. 8, a high frequency ac

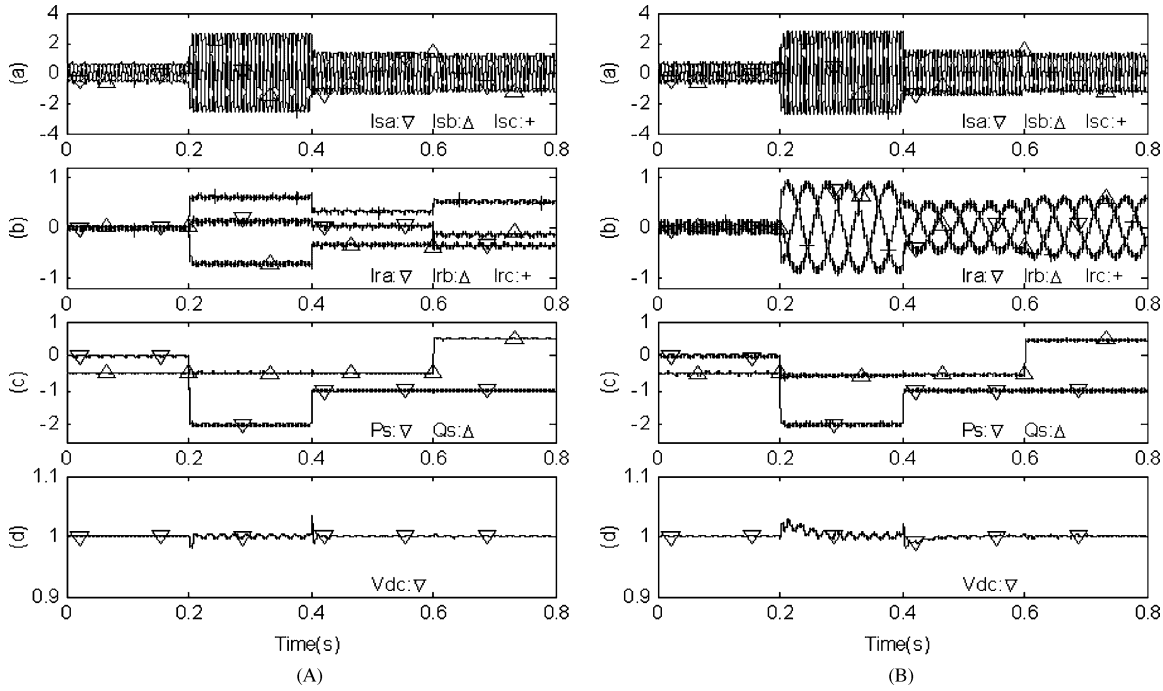

Fig. 9. Simulated results under various stator active and reactive power steps and constant rotor speed. (a) Three-phase stator current (kA). (b) Three-phase rotor current (kA). (c) Stator active power (MW) and reactive power (MVar). (d) dc link voltage (pu). (A) Rotor angular speed: 1.0 pu. (B) Rotor angular speed: 1.2 pu.

filter is connected to the stator side to absorb the switching harmonics generated by the two converters.

In a practical system, voltages and currents are sampled at the start of the sampling period. The required rotor control voltage for the sampling period is, then, calculated and passed to the PWM modulator. Inevitably, there is a time delay between the instant sampling and PWM modulator's receiving the required rotor control voltage. The proposed DPC strategy's rotor voltage calculation is relatively simple, and the time delay should be fairly small. Nevertheless, the simulated output rotor voltage is delayed by 50 μs to closely represent a practical DPC control system. During the simulation, the grid side converter is enabled first, such that the converter dc link voltage is regulated. The DFIG stator is, then, energized with the rotor rotating at a fixed speed, and with the rotor-side converter disabled. This starting process is not shown in the following results.

Initial studies with various active and reactive power steps were carried out to test the dynamic response of the proposed DPC strategy. The DFIG was assumed to be in speed control, i.e., with the rotor speed set externally, since in a practical system, the wind turbine's large inertia results in slow rotor speed change. Simulated results are shown in Fig. 9(A) and (B) for rotor speed of 1.0 and 1.2 pu, respectively, where the synchronous speed is defined as 1 unit. The rotor-side converter was enabled at 0.2 s with the initial stator active and reactive power references being -2 MW and -0.5 MVar, respectively ("$-$" refers to generating active power and absorbing reactive power). The active and reactive power references were step changed from -2 to -1 MW at 0.4 s and from -0.5 to $+0.5$ MVar at 0.6 s, respectively. The effectiveness of the proposed control strategy is clearly indicated in Fig. 9. The dynamic responses of both active and reactive powers are within a few milliseconds. The step change of one control variable, i.e., active or reactive power, does not affect the other due to the way the rotor voltage limit was applied. There is no overshoot of either the stator/rotor currents or the active/reactive powers.

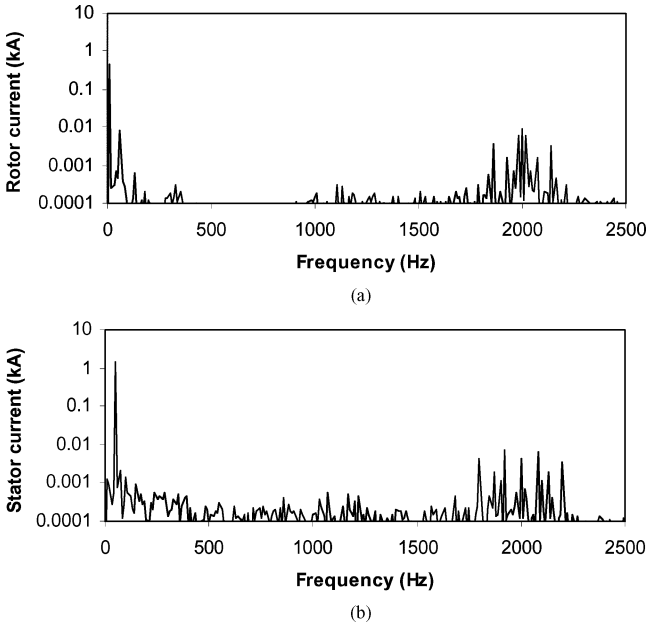

Fig. 10. Harmonic spectra of the rotor and stator current $\omega_r = 1.2$ pu, $P_s = 1.5$ MW, $Q_s = -0.5$ MVar). (A) Rotor current. (B) Stator current.

The harmonic spectra of the rotor and stator currents under the proposed DPC strategy are shown in Fig. 10(a) and (b),

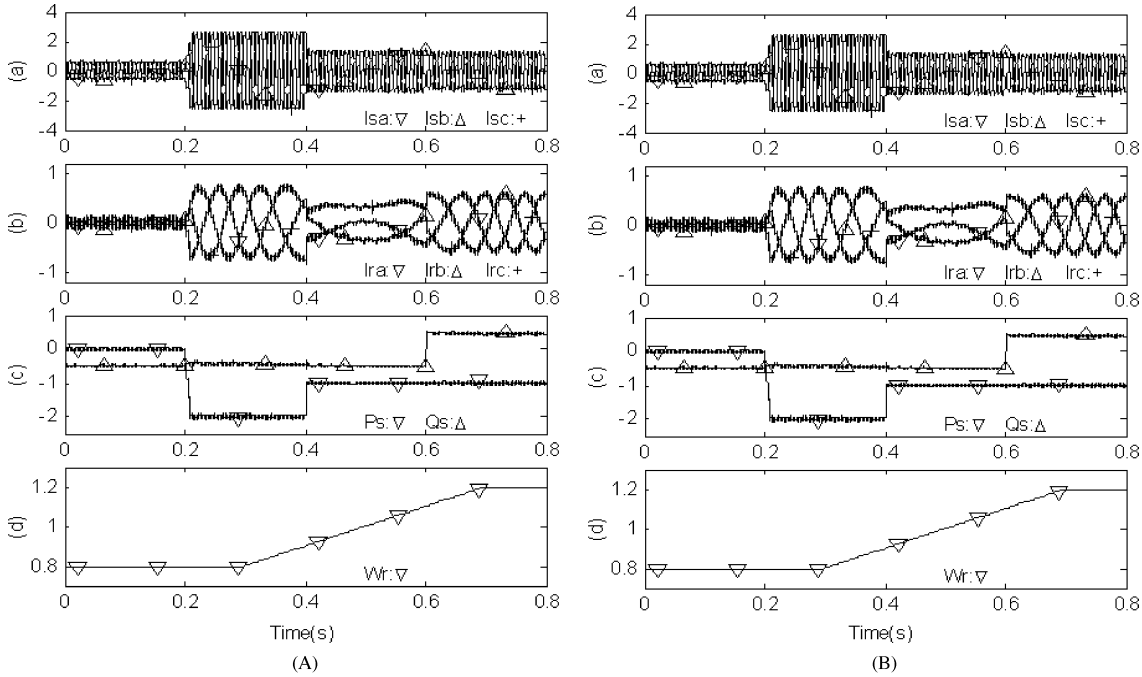

Fig. 11. Simulated results under various stator active and reactive power steps and rotor speed variation. (a) Three-phase stator current (kA). (b) Three-phase rotor current (kA). (c) Stator active power (MW) and reactive power (MVar). (d) Rotor speed (pu). (A) With nominal L_m. (B) With 20% L_m error.

respectively. The dominant harmonics for both currents are around the switching frequency of 2 kHz. For different operating conditions, such as different rotor speed and active and reactive powers, the system responses and current harmonic spectra were found to be similar to those shown in Figs. 9 and 10.

Studies with various power steps during rotor speed and machine parameter variations were carried out to further test the proposed DPC schemes. Fig. 11(A) and (B) shows the simulations with the mutual inductance used in the controller having 0% and 20% errors, respectively. As shown, during the period of 0.3–0.7 s, the rotor speed increased from 0.8 to 1.2 pu. Various power steps were applied, i.e., active and reactive power references were changed from -2 to -1 MW at 0.4 s, and from -0.5 to $+0.5$ MVar at 0.6 s, respectively. As seen in Fig. 11(A), the system response with rotor speed variation is satisfactory. Comparing Fig. 11(A) and (B), there is hardly any difference, and even with such large inductance errors, the system maintains superb performance under both steady-state and transient conditions.

The proposed DPC robustness was also tested with grid-side converter performance degraded to introduce significant dc voltage variation during transients. The impact of such dc voltage variation on the dynamic and steady-state performances of the proposed DPC strategy is negligible. The results are not shown here due to space limitations.

Further tests for a complete generation system including a typical 2 MW wind turbine and the DFIG were carried out. The DFIG was set in torque control, i.e., the speed is the result of stator/rotor voltage/current and the mechanical torque. The active power reference for the DFIG was calculated from the maximum power tracking curve [4]. Fig. 12 shows the simulated results when the wind speed changed from 11 to 13 m/s at 0.5 s, and then to 10 m/s at 1.5 s. The lumped inertia constant of the system is set to a relatively small value of 0.2 s in the study to reduce the simulation time. As can be seen from Fig. 12, the

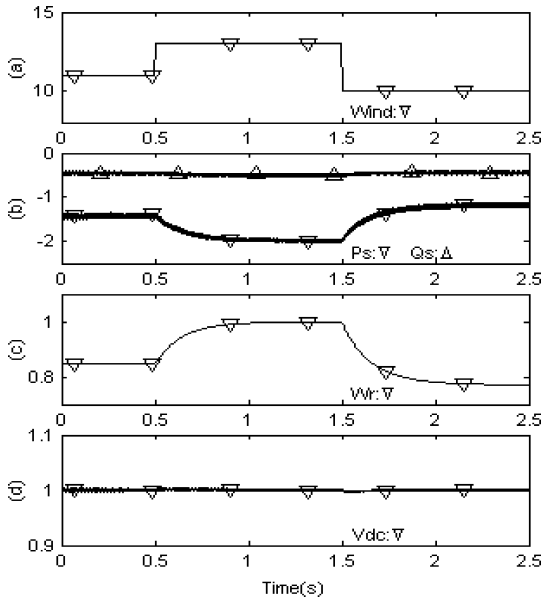

Fig. 12. Simulation results of a complete DFIG-based generation system with step change of wind speed. (a) Wind speed (m/s). (b) DFIG stator active and reactive power input (MVar). (c) Rotor speed (pu). (d) dc link voltage (pu).

TABLE I
PARAMETERS OF THE SIMULATED DFIG

Rated power	2MW
Stator voltage	690V
Stator/rotor turns ratio	0.3
R_s	0.0108pu
R_r	0.0121pu (referred to the stator)
L_m	3.362pu
$L_{\sigma s}$	0.102pu
$L_{\sigma r}$	0.11pu (referred to the stator)
Lumped inertia constant	0.2s
Number of pole pairs	2

system operation is satisfactory and maximum power tracking is achieved during wind speed variation.

V. CONCLUSION

This paper presented a new direct active and reactive power control strategy for a DFIG-based wind generation system. The controller directly calculates the required rotor control voltage within each fixed time period based on the stator flux, the rotor position, and the values of active and reactive powers and their errors. Constant converter switching frequency is achieved that eases the design of the power converter and the ac harmonic filter. Due to the relatively small power rating of the rotor-side converter, a method to limit the rotor voltage is proposed to improve the system transient performance. The impact of machine parameter variations on system response is analyzed and found to be negligible. Simulation confirms the effectiveness and robustness of the proposed DPC strategy during various operating conditions and variations of machine parameter.

APPENDIX

A. Parameters Affect the Rotor Voltage Vector Calculation

Considering $L_{\sigma s} \ll L_m$ and $L_{\sigma r} \ll L_m$, the constant k_σ and L_r/L_m can be simplified as

$$\begin{aligned} k_\sigma &= \frac{3}{2}\frac{L_m}{\sigma L_s L_r} = \frac{3}{2}\frac{L_m}{L_s L_r - L_m^2} \\ &= \frac{3}{2}\frac{L_m}{(L_{\sigma s}+L_m)(L_{\sigma r}+L_m) - L_m^2} \\ &= \frac{3}{2}\frac{L_m}{L_m(L_{\sigma s}+L_{\sigma r}) - L_{\sigma s}L_{\sigma r}} \\ &\approx \frac{3}{2}\frac{L_m}{L_m(L_{\sigma s}+L_{\sigma r})} = \frac{3}{2}\frac{1}{L_{\sigma s}+L_{\sigma r}} \end{aligned} \tag{A1}$$

$$\frac{L_r}{L_m} = \frac{L_{\sigma s}+L_m}{L_m} = 1 + \frac{L_{\sigma s}}{L_m}. \tag{A2}$$

B. Parameters of the DFIG Used for Simulation

See Table I for listing of the DFIG Parameters.

REFERENCES

[1] W. Leonhard, *Control of Electrical Drives*. London, U.K.: Springer, 2001.

[2] R. Pena, J. C. Clare, and G. M. Asher, "Doubly fed induction generator using back-to-back PWM converters and its application to variable-speed wind-energy generation," *Inst. Elect. Eng. Proc. Elect. Power Appl.*, vol. 143, no. 3, pp. 231–241, May 1996.

[3] H. Akagi and H. Sato, "Control and performance of a doubly-fed induction machine intended for a flywheel energy storage system," *IEEE Trans. Power Electron.*, vol. 17, no. 1, pp. 109–116, Jan. 2002.

[4] R. W. De Doncker, S. Muller, and M. Deicke, "Doubly fed induction generator systems for wind turbines," *IEEE Ind. Appl. Mag.*, vol. 8, no. 3, pp. 26–33, May/Jun. 2002.

[5] I. Takahashi and T. Noguchi, "A new quick-response and high-efficiency control strategy of an induction motor," *Inst. Elect. Eng. Trans. Ind. Appl.*, vol. 22, no. 5, pp. 820–827, 1986.

[6] M. Depenbrock, "Direct self-control (DSC) of inverter-fed induction machine," *IEEE Trans. Power Electron.*, vol. 3, no. 4, pp. 420–429, Oct. 1988.

[7] M. P. Kazmierkowski and A. Kasprowicz, "Improved direct torque and flux vector control of PWM inverter-fed induction motor drives," *IEEE Trans. Ind. Electron.*, vol. 42, no. 4, pp. 344–350, Aug. 1995.

[8] P. Vas, *Sensorless Vector and Direct Torque Control*. Oxford, U.K.: Clarendon, 1998.

[9] U. Baader, M. Depenbrock, and G. Gierse, "Direct self-control (DSC) of inverter-fed induction machine—A basis for speed control without speed measurement," *IEEE Trans. Ind. Appl.*, vol. 28, no. 3, pp. 581–588, May/Jun. 1992.

[10] D. Casadei, G. Grandi, G. Serra, and A. Tani, "Effects of flux and torque hysteresis band amplitude in direct torque control of induction machines," in *Proc. 20th Int. Conf. Ind. Electron., Control Instrum.*, 1994, pp. 299–304.

[11] T. G. Habetler, F. Profumo, M. Pastorelli, and L. M. Tolbert, "Direct torque control of induction machines using space vector modulation," *IEEE Trans. Ind. Appl.*, vol. 28, no. 5, pp. 1045–1053, Sep. 1992.

[12] Y. S. Lai and J. H. Chen, "A new approach to direct torque control of induction motor drives for constant inverter switching frequency and torque ripple reduction," *IEEE Trans. Energy Convers.*, vol. 16, no. 3, pp. 220–227, Sep. 2001.

[13] N. R. N. Idris and A. H. M. Yatim, "Direct torque control of induction machines with constant switching frequency and reduced torque ripple," *IEEE Trans. Ind. Electron.*, vol. 51, no. 4, pp. 758–767, Aug. 2004.

[14] J. Kang and S. Sul, "New direct torque control of induction motor for minimum torque ripple and constant switching frequency," *IEEE Trans. Ind. Appl.*, vol. 35, no. 5, pp. 1076–1082, Sep./Oct. 1999.

[15] T. Noguchi, H. Tomiki, S. Kondo, and I. Takahashi, "Direct power control of PWM converter without power-source voltage sensors," *IEEE Trans. Ind. Appl.*, vol. 34, no. 3, pp. 473–479, May/Jun. 1998.

[16] G. Escobar, A. M. Stankovic, J. M. Carrasco, E. Galvan, and R. Ortega, "Analysis and design of direct power control (DPC) for a three phase synchronous rectifier via output regulation subspaces," *IEEE Trans. Power Electron.*, vol. 18, no. 3, pp. 823–830, May 2003.

[17] M. Malinowski, M. P. Kazmierkowski, S. Hansen, F. Blaabjerg, and G. D. Marques, "Virtual-flux-based direct power control of three-phase PWM rectifiers," *IEEE Trans. Ind. Appl.*, vol. 37, no. 4, pp. 1019–1027, Jul./Aug. 2001.

[18] K. P. Gokhale, D. W. Karraker, and S. J. Heikkila, "Controller for a wound rotor slip ring induction machine," U.S. Patent 6 448 735 B1, Sep. 2002.

[19] L. Xu and P. Cartwright, "Direct active and reactive power control of DFIG for wind energy generation," *IEEE Trans. Energy Convers.*, vol. 21, no. 3, pp. 750–758, Sep. 2006.

[20] H. Akagi, Y. Kanazawa, and A. Nabae, "Generalized theory of the instantaneous reactive power in three-phase circuits," in *Proc. Int. Power Electron. Conf.*, 1983, pp. 1375–1386.

[21] H. W. Van De Broeck, H. C. Skudelny, and G. V. Stanke, "Analysis and realization of a pulsewidth modulator based on voltage space vectors," *IEEE Trans. Ind. Appl.*, vol. 24, no. 1, pp. 142–150, Jan./Feb. 1988.

[22] S. R. Bowes, "Advanced regular-sampled PWM control techniques for drives and static power converters," *IEEE Trans. Ind. Electron.*, vol. 42, no. 4, pp. 367–373, Aug. 1995.

[23] J. L. Thomas, S. Poullain, and A. Benchaib, "Analysis of a robust DC-bus voltage control system for a VSC-Transmission scheme," in *Proc. 7th Int. Conf. AC-DC Power Trans.*, London, U.K., 2001, pp. 119–124.

Dawei Zhi (S'07) received the B.Sc. and M.Sc. degrees in electrical and electronic engineering from Zhejiang University, Hangzhou, P. R. China, in 2000 and 2003, respectively. He is currently working toward the Ph.D. degree at Queen's University of Belfast, Belfast, U.K.

From 2003 to 2005, he was with Delta Power Electronics Center, Shanghai, China. His current research interests include power electronics, machine drives, and control and operation of DFIG for wind energy generation.

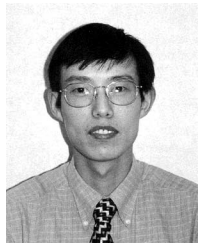

Lie Xu (M'03–SM'06) received the B.Sc. degree in electrical and electronic engineering from Zhejiang University, Hangzhou, China, in 1993, and the Ph.D. degree in electrical and electronic engineering from the University of Sheffield, Sheffield, U.K., in 1999.

From 1999 to 2000, he was with the Centre for Economic Renewable Power Delivery (CERPD), University of Glasgow, Glasgow, U.K., and from 2001 to 2003, he was with ALSTOM T&D, Stafford, U.K. He is now with the School of Electronic, Electrical Engineering and Computer Science, Queen's University of Belfast, Belfast, U.K. His current research interests include power electronics, renewable energy, and application of power electronics to power systems.